Chem

CellPress

Article

Ion-Solvent Chemistry-Inspired Cation-Additive Strategy to Stabilize Electrolytes for Sodium-Metal Batteries

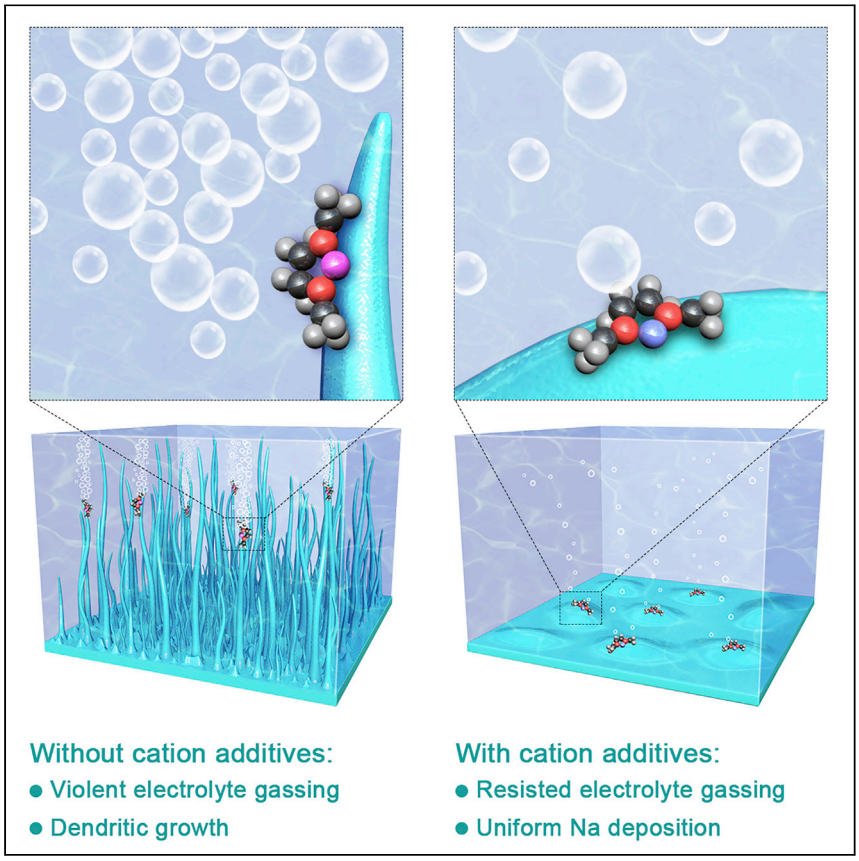

Building stable electrolytes is very essential for constructing stable sodium (Na) metal batteries as the reactive nature and the dendritic growth of Na metal anodes. Herein, we propose a paradigmatic and rational strategy of cation additive to stabilize electrolytes for Na metal batteries. The cation additive strategy affords emerging chances for rational electrolyte design for stable and safe Na metal batteries and is also applicable to other battery systems.

Xiang Chen, Xin Shen, Ting-Zheng Hou, Rui Zhang, Hong-Jie Peng, Qiang Zhang

zhang-qiang@mails.tsinghua.edu.cn

HIGHLIGHTS

The cation additive strategy was proposed for sodium metal batteries

Three principles were proposed to design cation additives

Cation additives can resist electrolyte gassing and sodium dendritic growth

The cation additive strategy is applicable to other battery systems

Chen et al., Chem 6, 2242–2256
September 10, 2020
https://doi.org/10.1016/j.chempr.2020.06.036

CellPress

Chem

Article

Ion-Solvent Chemistry-Inspired Cation-Additive Strategy to Stabilize Electrolytes for Sodium-Metal Batteries

Xiang Chen,[1,6] Xin Shen,[1,6] Ting-Zheng Hou,[2,3] Rui Zhang,[1] Hong-Jie Peng,[4] and Qiang Zhang[1,5,*]

SUMMARY

Building stable electrolytes is one of the key technologies for sodium (Na)-metal batteries as the reactive nature and the dendritic growth of Na-metal anodes. Herein, a paradigmatic and rational strategy of cation additive was proposed to stabilize electrolytes for Na metal batteries. Three principles, including the electrode potential of introduced cations, the lowest unoccupied molecular orbital energy level decrease of solvents after coordinating with cations, and the interaction strength between cations and solvents, were proved through first-principles calculations and molecular dynamics simulations. Li^+ was predicted to be a good cation additive candidate for Na metal batteries. Finite element method simulations, *in situ* optical microscopic observations, and electrochemical tests further validated the resisted Na dendritic growth due to the electrostatic shield effect and enhanced electrolyte stability after introducing Li^+ additives. The proven cation additive strategy affords emerging chances for rational electrolyte design for stable and safe Na metal batteries.

INTRODUCTION

Advanced battery technology plays an increasingly important role in modern society as the rapid development of electronic devices, electric vehicles, and smart grids.[1–4] The high-energy-density and safe energy storage system is strongly demanded worldwide. Lithium (Li)- and sodium (Na)- metal batteries have been revived recently due to their promising high energy density. Comparing with Li-metal batteries, Na-metal batteries are expected to be applied to large-scale energy storage considering the abundant resource and low expense of Na.[5,6] However, distinctive from conventionally applied carbon anodes, the introduction of Na-metal anodes puts forward much more stringent requirements for electrolytes as the high reactivity and dendritic-growth nature of Na metal.

Although solid-state batteries have attracted worldwide attention and achieved great progress in terms of the practicality of Na metal anodes,[7–9] the solid-solid interfacial issues remain and dendritic growth was observed,[10] which was likewise reported in solid-state Li-metal batteries.[11–13] Liquid electrolytes, therefore, still play an important role in the successful demonstration of Na metal batteries. Various strategies from the electrolyte side have been proposed to stabilize Na-metal-anode-electrolyte interface, including (co-)solvents, Na salts, and electrolyte additives. Specifically, compared with the widely used ester solvents in Li-ion batteries, such as ethylene carbonate (EC) and diethyl carbonate (DEC), ether solvents, such as 1,2-dimethoxyethane (DME), are more widely applied in Li- and Na-metal batteries

The Bigger Picture

Building stable electrolytes is very essential for constructing stable sodium (Na) metal batteries as the reactive nature and the dendritic growth of Na metal anodes. Herein, we propose a paradigmatic and rational strategy of cation additive to stabilize electrolytes for Na metal batteries. Three principles are suggested to theoretically screen cation additives, which are further validated by experiments. The proven cation additive strategy affords emerging chances for rational electrolyte design for stable and safe Na metal batteries and is also applicable to other battery systems.

due to their lower reduction potential and better stability against metal anodes. Numerous Na salts[14,15] have been used for Na-metal batteries, such as Na bis(fluorosulfonyl)imide (NaFSI), Na bis-(trifluoromethane sulphonyl)imide (NaTFSI), Na hexafluorophosphate ($NaPF_6$), and Na difluoro(oxalato)borate (NaDFOB). The decomposition of salt anions can regulate the composition and structure of solid-electrolyte interphase (SEI) on anodes and therefore stabilize the anode-electrolyte interface.

The choice of electrolyte additives is even more diverse, which can be mainly categorized into three classes. First, small neutral molecules, such as fluoroethylene carbonate (FEC)[16–18] and water.[19] Second, anion additives that afford the same cation but different anions comparing with the added salt, such as $NaNO_2$[20] and $NaNO_3$.[21] Third, cation additives that provide the same anion but different cations compared with the salt. This strategy was first demonstrated in Li-metal batteries by Zhang and co-workers in 2013.[22] While the first two categories of electrolyte additives have been widely investigated for Na-metal batteries,[16–21] the prospect of cation additives is much less explored and the role of cation additive in electrolytes is not fully understood yet. Therefore, it is of great importance to investigate the role of cation additives in electrolytes, including the electrostatic shield effect, the regulation of electrolyte solvation structures, and the effect on electrolyte stability. Based on these understandings, fundamental principles can be built to rationally design cation additives to achieve a stable and safe battery.

In this contribution, a paradigmatic and rational strategy of cation additive inspired from ion-solvent chemistry was established for Na metal batteries. A series of cation additives (Li^+, K^+, Mg^{2+}, Ca^{2+}, Cu^{2+}, Zn^{2+}, and Al^{3+}) were investigated for $NaPF_6$-DME-based electrolytes, which was previously proved to render good compatibility with Na-metal anodes.[15] The regulation of cation additive on electrolyte stability and electrolyte solvation structure was investigated through first-principles calculations. Molecular dynamics (MD) simulations confirmed the electrolyte solvation structures after introducing cation additives. Finite element method (FEM) simulations, *in situ* optical microscopic observations, and electrochemical tests further validated the cation additive strategy predicted by density functional theory (DFT) and MD calculations. This work establishes a general principle of designing cation additives for Na-metal batteries, which also provides a research paradigm for other rechargeable batteries. The strategy of cation additive affords emerging chances for designing stable electrolytes against reactive metal anodes and resisting dendritic growth.

RESULTS

Thermodynamic Analyses and Design Principles

The following screening rules are suggested for the rational design of cation additives into electrolytes for Na metal batteries:

(1) According to ion-solvent chemistry, the formation of cation-solvent complex can promote the decomposition of electrolyte on Na-metal anodes and the effects of different cations are different.[23,24] Hence, it is necessary that the newly introduced cation-solvent complex is more stable than Na^+-solvent complex. Otherwise, the electrolyte decomposition on Na-metal anodes will be promoted.
(2) In order to resist the growth of Na dendrites, the cation additive should not be reduced and therefore has an electrostatic shield effect on Na deposition.

[1]Beijing Key Laboratory of Green Chemical Reaction Engineering and Technology, Department of Chemical Engineering, Tsinghua University, Beijing 100084, China

[2]Department of Materials Science and Engineering, University of California Berkeley, 210 Hearst Mining Building, Berkeley, CA 94720, USA

[3]Energy Technologies Area, Lawrence Berkeley National Laboratory, Berkeley, CA 94720, USA

[4]Department of Chemical Engineering, Stanford University, Stanford, CA 94305, USA

[5]These authors contributed equally

[6]Lead Contact

*Correspondence: zhang-qiang@mails.tsinghua.edu.cn

https://doi.org/10.1016/j.chempr.2020.06.036

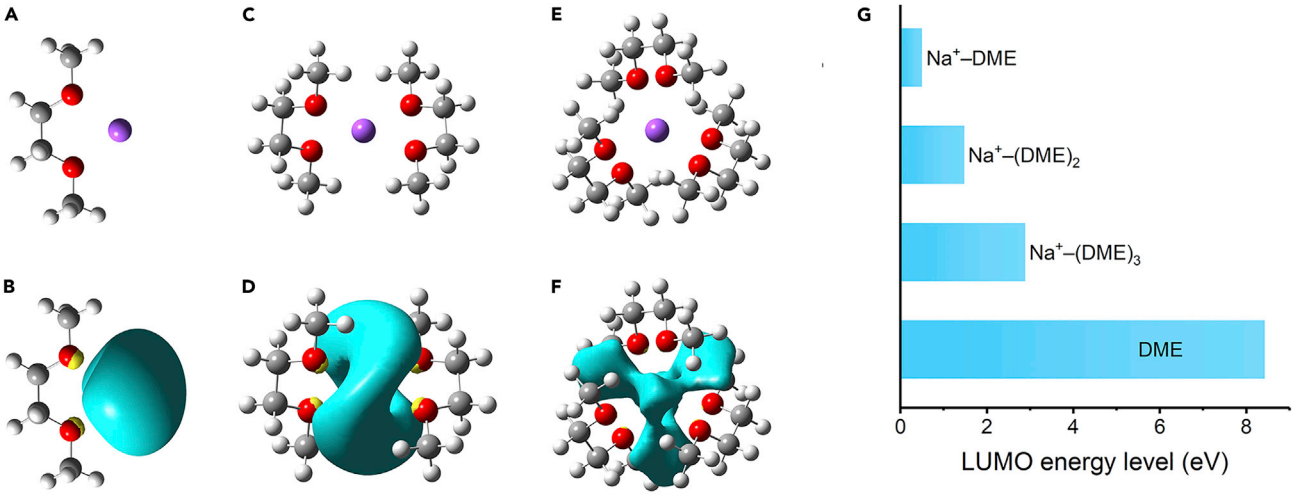
A
C
E
G
B
D
F
Na+–DME
Na+–(DME)2
Na+–(DME)3
DME
0
2
4
6
8
LUMO energy level (eV)

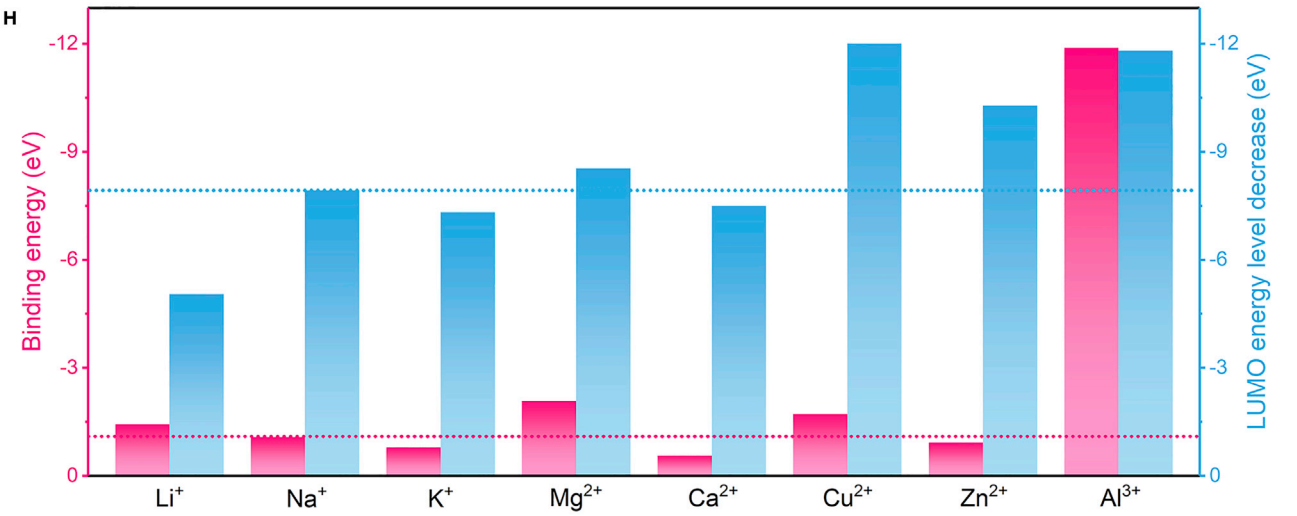
H
Binding energy (eV)
LUMO energy level decrease (eV)
-12
-9
-6
-3
0
Li+
Na+
K+
Mg2+
Ca2+
Cu2+
Zn2+
Al3+

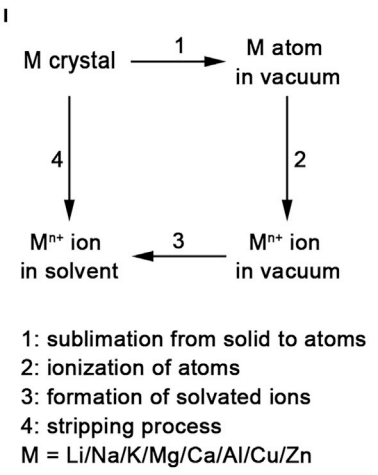
I
M crystal
1
M atom
in vacuum
4
2
Mn+ ion
in solvent
3
Mn+ ion
in vacuum
1: sublimation from solid to atoms
2: ionization of atoms
3: formation of solvated ions
4: stripping process
M = Li/Na/K/Mg/Ca/Al/Cu/Zn

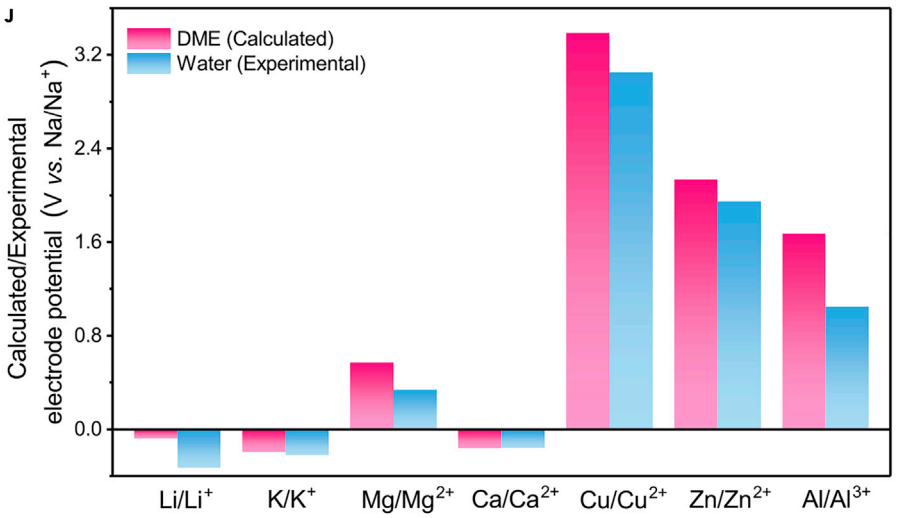
J
DME (Calculated)
Water (Experimental)
Calculated/Experimental electrode potential (V vs. Na/Na+)
3.2
2.4
1.6
0.8
0.0
Li/Li+
K/K+
Mg/Mg2+
Ca/Ca2+
Cu/Cu2+
Zn/Zn2+
Al/Al3+

Figure 1. Thermodynamic Analyses of Cation Additives

(A–F) The geometrical structure and the isosurface of LUMO of Na^+–$(DME)_n$ complexes. Geometrical structures: (A) Na^+–DME, (C) Na^+–$(DME)_2$, and (E) Na^+–$(DME)_3$. LUMO isosurface: (B) Na^+–DME, (D) Na^+–$(DME)_2$, and (F) Na^+–$(DME)_3$. The hydrogen, carbon, oxygen, and sodium atoms are marked with white, gray, red, and purple, respectively. The cyan and yellow regions represent the positive and negative parts of the LUMO isosurface, respectively (isovalue: 0.03).

(G) The comparison of LUMO energy level of Na^+–$(DME)_n$ complexes and DME.

(H) The comparison of LUMO energy level decreases and binding energy of ion–DME complexes.

(I) The thermodynamic cycle of calculating electrode potential.

(J) The calculated or experimental electrode potential of the considered metal/cation pairs.

Although some cations can be reduced to form an alloy layer on Na-metal anodes and therefore stabilize the electrolyte-anode interface. The formation of the alloy layer cannot block the electron transfer from anodes to electrolytes completely and cation additives will be consumed continuously. Besides, the performance of the alloy layer highly depends on its solid phase properties, which is beyond the scope of the current work. Therefore, a lower electrode potential than Na/Na^+ is enforced for cation additives.

(3) Cation additives that have a larger binding energy than Na^+-solvent are preferred. A lower electrode potential than Na/Na^+ is not sufficient to ensure preferred Na ions reduction. Additive cations are still possible to be reduced due to rapid solvation-desolvation kinetics compared with Na. Therefore, cations with a larger binding energy with solvent molecules are needed where a larger desolvation barrier and a more sluggish reduction kinetics will guarantee the unfavored reduction of the co-cation. Moreover, the stronger affinity with solvents yields a good solubility of the cation. Among the three screening rules of co-cations, the former two rules should be prioritized since the binding energy between cations and solvents cannot be well quantified and is an incomplete abstraction for the nucleation kinetic issues.

In order to probe the regulation of cations on solvent-reductive stability, cation-solvent complex model is adopted herein (Figures 1A–1F). For instance, one Na^+ can coordinate with one, two, or three DME molecules according to the MD simulation results. When Na^+ is complexed with one DME, the energy level of the lowest unoccupied molecular orbital (LUMO) of DME is reduced by −7.93 eV (Figure 1G and Table S1). A lower-energy-level LUMO indicates the cation-solvent complex is able to obtain electrons from anode and therefore be reduced more easily. Besides, the coordination of the solvent with Na^+ also increases the C–O bond length from 1.418 and 1.1421 to 1.434 and 1.437 Å (carbon atom in methyl and methylene functional group, Table S2). The C–O bond was predicted to break preferentially when DME decomposed on metal anodes and a stretched bond length can promote such decomposition reactions.[25] Therefore, a smaller amount of LUMO energy decrease is preferred when the cation-solvent coordination happens, and the LUMO energy decrease value is selected to quantify the relative stability between solvation structures in rule (1). It is noted that when Na^+ is coordinated with more than one DME molecule, such influence is weakened. Na^+ can reduce LUMO level by −6.95 and −5.54 eV in Na^+–$(DME)_2$ and Na^+–$(DME)_3$, respectively. As more DME coordinated, the interaction between Na^+ and DME is weakened and Na^+ has a less significant impact on LUMO level. However, this trend is not always true for other cations (Figures S1–S7). For instance, in the case of Li^+, the Li^+–DME, Li^+–$(DME)_2$, and Li^+–$(DME)_3$ complexes show very similar LUMO energy level, 3.37, 3.61, and 3.44 eV, respectively (Figure S1); in the case of Cu^{2+}, Cu^{2+}–$(DME)_2$ exhibits a much lower LUMO level (−8.13 eV) than that of Cu^{2+}–DME(−3.59 eV) and Cu^{2+}–$(DME)_3$ (−7.21 eV).

The comparison of the LUMO energy level decrease and binding energy is presented in Figure 1H (M–DME complexes), S8 (M–$(DME)_2$ complexes), and S9 (M–$(DME)_3$ complexes) to select proper cation additives for Na-metal batteries (Table S3). In all cases, only Li^+ and K^+ exhibit a smaller decrease in the LUMO level of DME compared with Na^+. Ca^{2+} satisfies this rule only in M–DME complex and Al^{3+} satisfies this rule in M–$(DME)_2$ and M–$(DME)_3$ complexes (M = Li^+, K^+, Mg^{2+}, Ca^{2+}, Cu^{2+}, Zn^{2+}, and Al^{3+}).

Furthermore, the electrode potential of considered metals was investigated (Figures 1I and 1J). Since the electrolyte solvation has a significant influence on electrode potential of cations, the electrode potential in DME electrolytes was calculated based on theoretical methods, in which the experimental cohesive energy and calculated ionization energy-solvation energy were used (more details in the part of First-Principles Calculations). Li/Li^+ exhibits the lowest electrode potential (−0.33 V versus Na/Na^+ or −3.04 versus standard hydrogen electrode) in the water system and the third lowest in DME (−0.08 V versus Na/Na^+) among the considered metal electrodes. K/K^+ and Ca/Ca^{2+} also exhibit a lower electrode potential than Na/Na^+ in water and DME. The above results highlight the important role of electrolyte solvation in determining the metal-cation electrode potential, which agrees with previous experimental reports that K^+ has a higher standard redox potential in water but a lower redox potential in EC/DEC (v/v = 1:1) electrolytes than Li^+.[26,27]

Considering cation additives should have a lower electrode potential than Na-metal anodes, Li^+, K^+, and Ca^{2+} are suggested herein. With an overall consideration with the LUMO level decrease and the binding energy discussed above, Li^+ is expected to be the most outstanding candidate. Li^+ has an electrode potential of −0.08 V versus Na/Na^+, which can hardly become positive (Table S4) given that the concentration of additives is typically much smaller than the working ions in a practical cell. What is more, Li^+ has a larger binding energy with DME molecule than Na^+, making it more difficult to be desolvated. Therefore, Li ions cannot be reduced on Na-metal anodes. More importantly, Li^+ reduces the LUMO level of DME less than Na^+, which can stabilize the electrolyte solvents against Na-metal anodes.

Molecular Dynamics Analyses and Electrolyte Solvation Structure

As proved in the above part, Li^+ cation additive is expected to stabilize electrolytes for Na-metal batteries. The influence of Li ions on electrolyte properties was further probed by MD simulations. Four models were considered, including 0.50 M $NaPF_6$ DME, 1.00 M $NaPF_6$ DME, 1.00 M $NaPF_6$ + 0.50 M $LiPF_6$ DME, and 1.50 M $NaPF_6$ DME (Figures 2A, 2B, S10, and S11). The ratio of DME coordinated with cations is mainly determined by the concentration of salts in electrolytes as both Li^+ and Na^+ have a very close coordination number around six. The ratios are 9.42%, 18.18%, 25.65%, and 27.60% for 0.50 M $NaPF_6$ DME, 1.00 M $NaPF_6$ DME, 1.50 M $NaPF_6$ DME, and 1.00 M $NaPF_6$ + 0.50 M $LiPF_6$ DME electrolytes, respectively. With the increase of salt concentration, large aggregates form and are connected by PF_6^- anions (e.g., Figure S10 versus S11).

In order to quantitatively analyze the solvation structure, radial distribution function g(r) analyses were conducted (Figures 2C, 2D, S12, and S13) and the summary of Na coordination number with O/F in different electrolytes is presented in Figure 2E. The g(r) profiles of Na–O and Na–F shows dominant peaks at around 2.25 and 2.19 Å, respectively, which indicate the first solvation shell of Na^+ (Figure 2C). The peaks of Na–F g(r) profile at around 4.13 and 5.37 Å are assigned to F atoms of PF_6^- anions that are not directly bonded with Na^+ in the first solvation shell. When Li^+ was

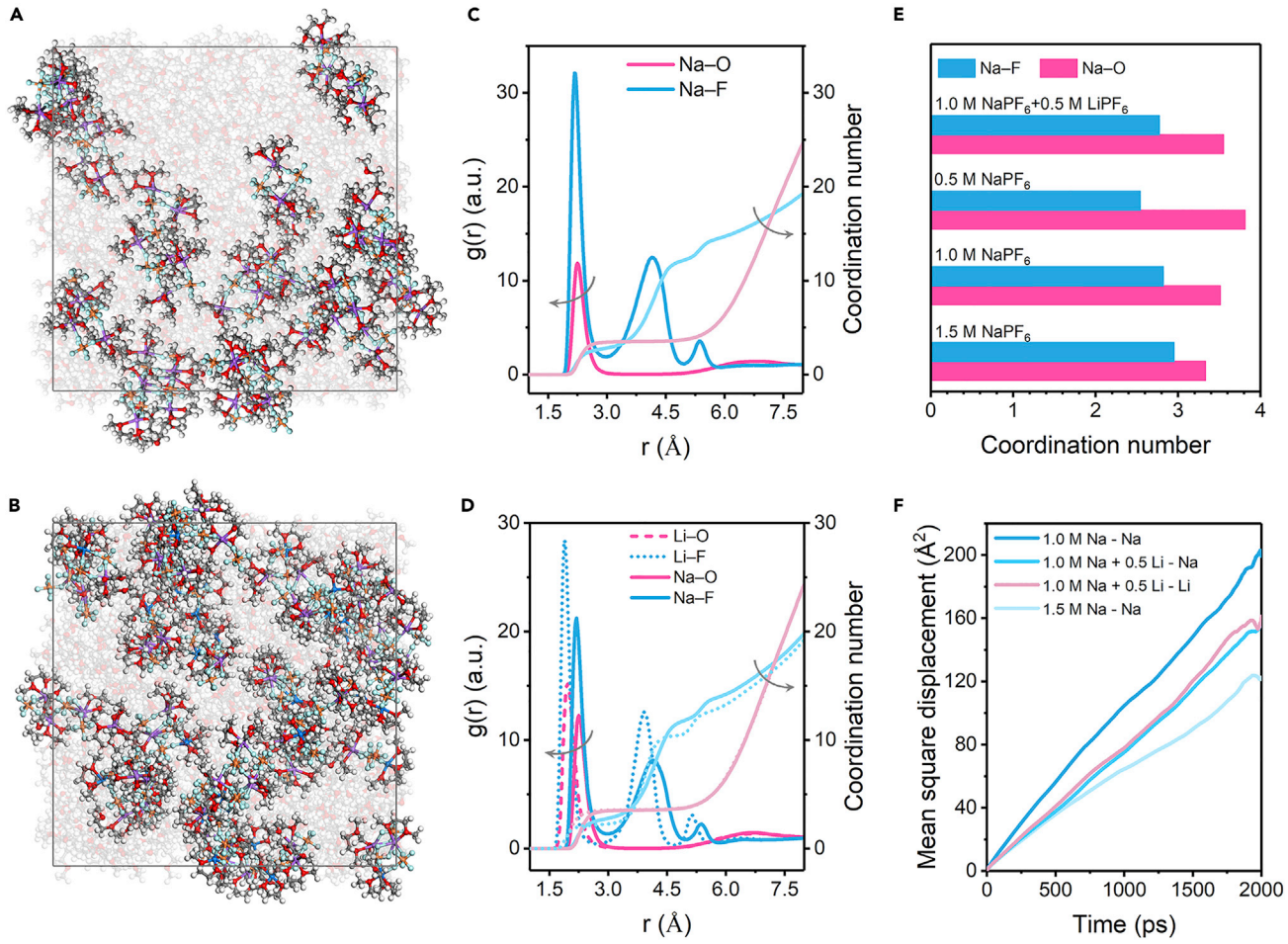

Figure 2. Molecular Dynamics Simulation Analyses of Cation Additives

(A and B) The simulated geometrical structure of (A) 1.00 M $NaPF_6$ DME and (B) 1.00 M $NaPF_6$ + 0.50 M $LiPF_6$ DME electrolytes. The hydrogen, lithium, carbon, oxygen, fluorine, sodium, and phosphorus atoms are marked with white, blue, gray, red, light blue, purple, and orange, respectively. Solvents that are not coordinated with Li or Na are marked translucent.

(C and D)The radial distribution function g(r) analyses of (C) 1.00 M $NaPF_6$ DME and (D) 1.00 M $NaPF_6$ + 0.50 M $LiPF_6$ DME electrolytes.

(E) The summary of the coordination number of Na with O/F atom in different electrolyte models.

(F) The mean square displacement of Li and Na ions in different model electrolytes.

introduced into the electrolytes, the solvation sheath of Li^+ is similar with Na^+ (Figure 2D). As the radius of Li^+ is smaller than Na^+ radius, the Li–O and Li–F pairs exhibit shorter characteristic distances of around 1.97 and 1.89 Å, respectively. In order to evaluate the influence of Li^+ on the solvation structure of Na^+, the coordination number of Na^+ with O/F was compared for electrolytes with or without $LiPF_6$ (Figure 2E). First, the solvation structure of Na^+ can be greatly influenced by salt concentration. Comparing high-concentration electrolytes (1.50 M) with low-concentration electrolytes (0.50 M), the coordination number of Na^+ with O is decreased from 3.81 to 3.33. Simultaneously, the coordination number of Na^+ with F is increased from 2.54 to 2.95. Therefore, Na^+ in high-concentration electrolytes is more likely to coordinate with PF_6^- than Na^+ in low-concentration electrolytes, which agrees with that large clusters form in high-concentration electrolytes. Comparing 1.00 M $NaPF_6$ + 0.50 M $LiPF_6$ electrolyte with 1.00 M $NaPF_6$ electrolyte, the coordination number of Na^+ with O is slightly increased from 3.51 to 3.55 and the coordination number of Na^+ with F is slightly decreased from 2.82 to 2.77. Consequently, the introduced

Li^+ has an insignificant influence on the solvation structure of Na^+ in the presence of largely excess DME solvents. Li^+ and Na^+ are solvated as much as possible without competition in low-concentration electrolytes. However, it should be noted that this is the bulk property and the solvation structure of cations on the surface of anodes can be different. The latter is largely determined by the electrode surface structures, similar to the formation of electrical double layer. Comparing with Na ions, Li ions can deliver a larger binding energy toward the nucleophilic sites and consequently are enriched on the electrode surface. Besides, polynuclear cationic associates can be formed on the anode-electrolyte interface due to the competition between Li and Na ions.[28]

In addition to solvation structure, the transport property of cations in electrolytes was further analyzed by calculating the mean square displacement (Figure 2F). The diffusion rate of cations in electrolytes can be mainly influenced by two factors: the size of formed solvated cations and the interaction strength between cations and solvents.[27] Solvated cations with a small radius are supposed to move faster with their solvation shell (vehicular diffusion) than cations with a large solvation radius. Meanwhile, cations can shuttle through the solvent network (structural diffusion) by exchanging coordinated solvents with free solvents quickly if the binding energy between cations and solvents is small. Considering these two factors, Li^+ can form a smaller-radius solvation structure but possibly a stronger interaction with solvents compared with with Na^+. Therefore, the comparison of Li^+ and Na^+ diffusivity in electrolytes is highly dependent on solvents, temperature, salts, etc.[29–32] In our investigated case at room temperature, Li^+ and Na^+ have a very close diffusivity in DME solvents (Figure S14) and the cation diffusivity is mainly influenced by salt concentration (Figure 2F). In a high-concentration electrolyte, large solvation structures are formed, which decreases the cation diffusivity. Specifically, the self-diffusion coefficient of Na^+ is reduced from 1.59×10^{-10} to 9.79×10^{-11} m^2 s^{-1} when the concentration of $NaPF_6$ is increased from 1.00 to 1.50 M. In the mixture electrolyte of 1.00 M $NaPF_6$ + 0.50 M $LiPF_6$, Na^+ and Li^+ have a close diffusivity due to their similar diffusion properties in DME electrolytes. The self-diffusion coefficient of Na^+ in the mixture electrolyte is 1.29×10^{-10} m^2 s^{-1}, which is smaller than that in 1.00 M $NaPF_6$ electrolyte but larger than that in 1.50 M $NaPF_6$ electrolyte. Therefore, the introduction of cation additives can better maintain the diffusivity of Na^+ in electrolytes than adding the same amount of Na^+, and a fine-tuned concentration of cation additives can be leveraged to benefit the anode-electrolyte interface with a controlled negative effect on the bulk electrolyte.

FEM Simulations and Experimental Validations

In order to prove the electrostatic shield effect of cation additives on Na depositions, FEM simulations and *in situ* optical microscopic observations were conducted (Figure 3). During FEM simulations, a semi-ellipse shape Na metal was set as the initial morphology. The semi-ellipse Na tends to mainly grow on the protuberance tip considering that this region exhibits a strong electrical field and more Na will be preferentially deposited around the tip rather than smooth regions of the anode (Figure 3A), which is similar with Li nucleation.[22] After introducing Li^+ additives, Li^+ is enriched on the tip of the semi-ellipse Na protuberance and cannot be reduced to Li metal due to a lower electrode potential than Na. The enriched Li^+ induces a strong electrostatic shield effect on Na^+, forcing Na^+ to deposit on the smooth region of anodes (Figure 3B). Consequently, Na is likely to grow smoothly and Na dendrite growth is restrained.

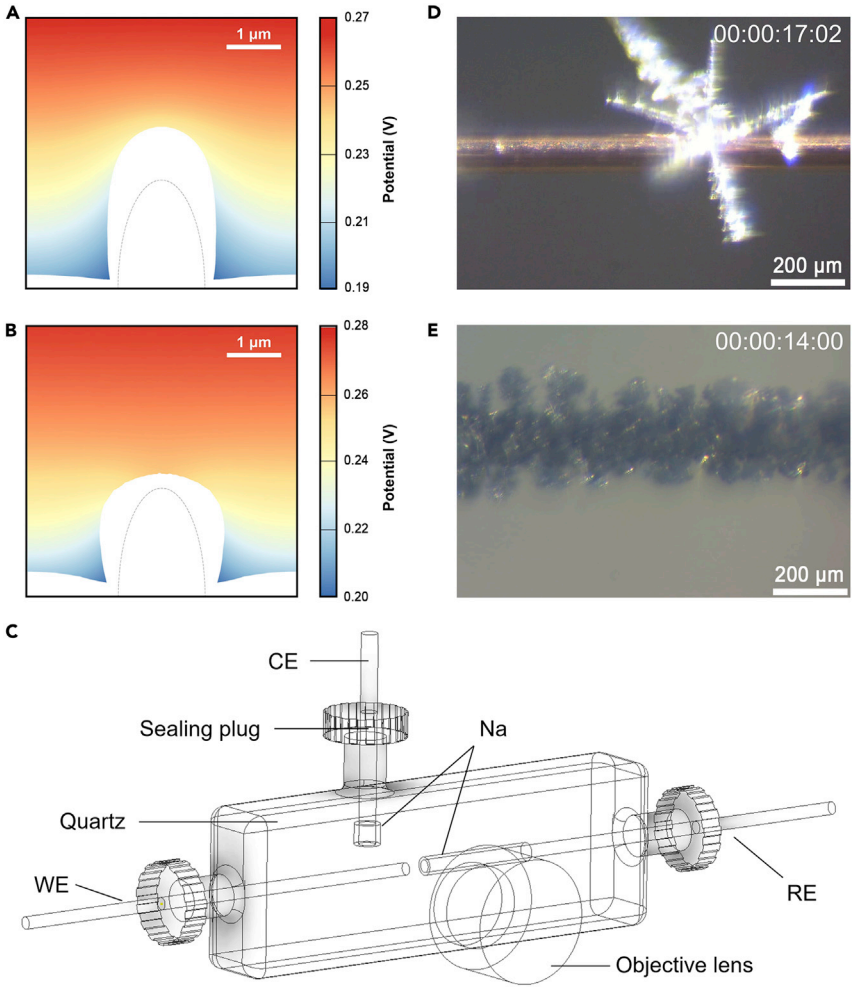

Figure 3. FEM Simulations and *In Situ* Optical Microscopic Observations

(A and B) The potential distribution of Na deposition in (A) 1.00 M $NaPF_6$ DME and (B) 1.00 M $NaPF_6$ + 0.50 M $LiPF_6$ DME electrolytes. The white area represents initial (within the gray semi-ellipse line) or deposited (outside the gray semi-ellipse line) Na metal.

(C) Schematic illustration of the home-made optical cell. WE, working electrode; CE, counter electrode; RE, reference electrode.

(D and E) *In situ* optical microscopic observations of Na deposition on copper wire in (D) 1.00 M $NaPF_6$ DME and (E) 1.00 M $NaPF_6$ + 0.50 M $LiPF_6$ DME electrolytes. The deposition current density was set to be 3.0 mA cm^{-2}.

In situ optical microscopic characterizations further prove such electrostatic shield effect of cation additives on Na deposition. In 1.00 M $NaPF_6$ DME electrolyte, Na deposit exhibits a needle-like shape (Figure 3D; Video S1), illustrating that Na^+ prefers to nucleate on tips and forms Na dendrites. The interaction between deposited Na and Cu substrate is weak due to insufficient contact, which can even cause the escaping of Na deposits from Cu substrates to electrolytes and form "dead" Na (Video S1). When 0.50 M $LiPF_6$ is introduced, the Na deposition shows a smooth morphology (Figure 3E; Video S2), disparate from needle-like Na dendrites. The electrostatic shield effect on inhibiting Na dendrite growth is therefore validated experimentally. Moreover, electrolyte gassing on Na dendrites was observed in 1.00 M $NaPF_6$ DME electrolyte, while it was much weakened after introducing Li^+

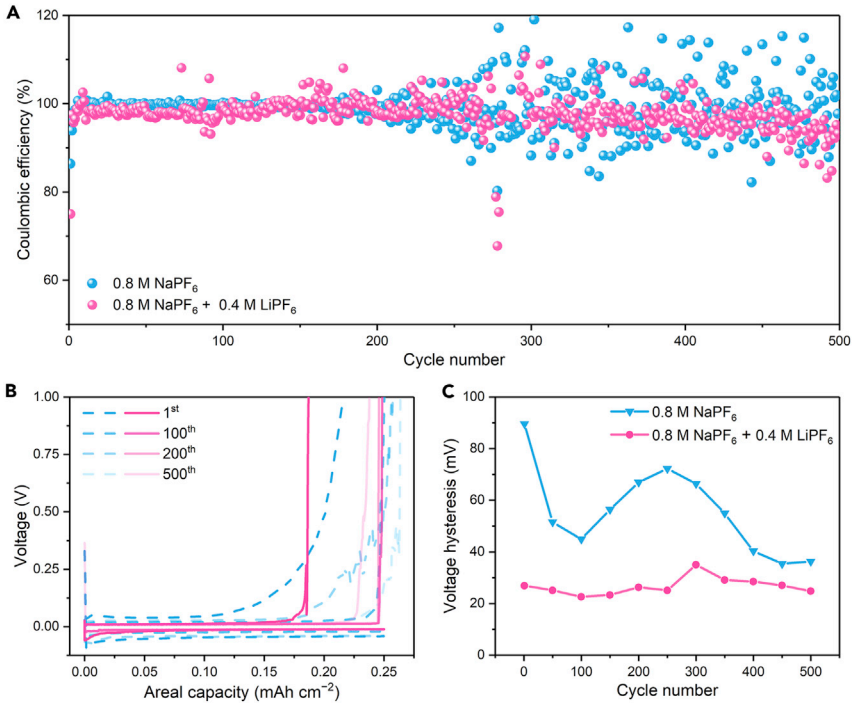

Figure 4. Electrochemical Tests of Cation Additive Strategy

(A) Coulombic efficiency of Na–Cu half cells.

(B) Voltage profiles of the 1st, 100th, 200th, and 500th cycle of Na–Cu half cells.

(C) Voltage hysteresis of the Na–Cu half cells. Current density: 0.25 mA cm^{-2}. Specific capacity: 0.25 mAh cm^{-2}.

additives (Videos S1 and S2), which is ascribed to the enhanced electrolyte stability on Na surface as Li^+–DME complexes are more stable than Na^+–DME complexes.

Electrochemical tests were further conducted to prove the practical performance of Li^+ additive in Na-metal batteries (Figure 4). In the Na–Cu half cell with the 0.80 M $NaPF_6$ DME electrolyte, the Coulombic efficiency can keep steady only around 200 cycles (Figure 4A). With Li^+ additive, the Coulombic efficiency after 200 cycles can be significantly improved. More importantly, the Li^+ additive can significantly reduce the voltage hysteresis, which is the sum of Na deposition overpotential and stripping overpotential (Figures 4B, 4C, and S15). For example, the voltage hysteresis of the first cycle can be reduced from 89.6 to 26.9 mV. In the following cycles, Li^+ additive can still render a much smaller and steadier voltage hysteresis comparing with electrolytes only containing Na^+, which is ascribed to the stable anode–electrolyte interface. Besides, the Li^+ additive also has an obvious influence on the Na stripping behavior. Without Li^+ additive, the Na stripping overpotential becomes larger as charging, which can be explained by the large mount of Na dendrites or "dead" Na (Figure 4B). The stripping of the Na with a low electrochemical reactivity requires a large overpotential. When Li^+ additive is introduced, a stable anode-electrolyte interface can form and less Na dendrite or "dead" Na will be produced. As a result, the charging voltage will increase sharply as long as the active Na is exhausted. These results agree with the *in situ* optical microscopic observations. Therefore, the effect of the cation additive strategy in batteries is validated.

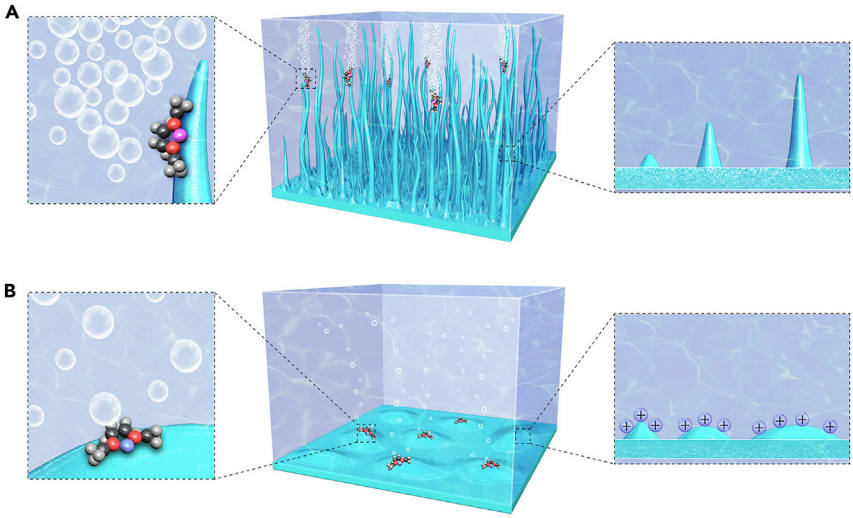

Figure 5. Schematic Diagrams of the Role of Cation Additives

(A) The electrolyte without cation additives. The electrolyte gassing is violent and the anode exhibits a dendritic morphology.

(B) The electrolyte with cation additives. The electrolyte gassing is prohibited to some degree and the anode exhibits a smooth morphology due to the electrostatic shield effect.

DISCUSSION

Extending of Cation Additive Strategy

The design strategy and functions of cation additives in Na metal batteries have been proved through first-principles calculations, MD simulations, FEM simulations, *in situ* optical microscopic observations, and electrochemical tests. The introduction of proper cation additives can stabilize anode-electrolyte interface and resist the growth of Na dendrites (Figure 5). This effective strategy is also supposed to be applied to other batteries. Especially, hybrid ion batteries (HIB), in which more than one cation exists in electrolytes, has attracted increasing attention recently.[33–36] While prior studies about HIB are mostly focused on electrode materials design, the electrolyte design is less addressed. Therefore, it is of great importance to investigate electrolytes with multications, where the electrolyte solvation structure, electrolyte stability, and cation intercalation and deintercalation behavior can be different from mono-cation electrolytes. The established cation additive principles for Na-metal batteries in the present work offer an emerging research paradigm for studying the multi-cation electrolyte for HIB.

Beyond Na batteries, the possible candidates for batteries with other metal anode materials are further analyzed according to the current results of DME electrolytes. Unfortunately, there is no suitable cation additive candidate among our considered cations for Li, K, and Al batteries (Figures 1H, 1J, S8, and S9). In the case of Li batteries, the decrease of electrolyte stability is the least significant with Li^+ and Li also has a low electrode potential, preventing any feasible cation additive. Meanwhile, K has the lowest electrode potential in DME electrolyte among the considered metals, which prohibits the inclusion of co-cations. Likewise, no other cation can form more stable complexes than Al^{3+} in all the M–DME, M–$(DME)_2$, and M–$(DME)_3$ cases. As for Mg batteries, Li^+ and K^+ are possible cation additives in the sense that they have a lower electrode potential and a less significant influence on decreasing electrolyte stability compared with Mg^{2+}. However, they all have a smaller binding energy toward DME than Mg^{2+}. It turns out that the Ca and Zn

batteries are the only battery systems that have co-cations surviving after enforcing the screening rules. K^+ exhibits a lower electrode potential and a less significant influence on reducing LUMO energy level of DME compared with Ca^{2+}. Therefore, K^+ is considered as a possible cation additive for Ca batteries. For Zn batteries, Mg^{2+} satisfies all the principles and is regarded as the best choice for cation additives. Li^+, Na^+, and K^+ satisfy the stability principle but they have a smaller binding energy toward DME than Zn^{2+}.

Model Evaluations

It should be noted that all these results are based on DME electrolytes, which are mostly applied in alkali-metal-based rechargeable batteries. However, Mg, Ca, and Zn batteries typically employ carbonate or sulfone electrolytes. The regulation can be totally different in various solvents as electrolyte solvation plays an important role in regulating electrolyte component interactions.[37] First, the metal electrode potential is highly dependent on electrolytes. As shown in Figure 1J, the electrode potential exhibits different trends in DME and water systems. For instance, Li has a lower electrode potential in the water system but a higher electrode potential in DME system compared with K. Second, the effect of cation on reducing LUMO level of solvents is also contingent upon solvents. As discussed in our previous work, the origins of such effect in ether and ester solvents are different from each other.[23] Furthermore, the dendrite growth is less considered an issue for Mg batteries.[38] Consequently, the standards for selecting cation additives should be tailored on a case-by-case basis in various battery systems.

The influence of anions on solvation structure was also neglected in the current model. Cations are mainly coordinated with solvents in dilute electrolytes, while the ratio of anions in cation solvation structure enlarges as there is increase in electrolyte concentration.[39] Therefore, in high-concentration electrolytes, which were proved to be effective for both Na- and Li-metal batteries,[40–43] anions can regulate the interaction between cations and solvents. The stability of solvents is therefore influenced by the coordinated anions, i.e., the coordinated anions can also affect the electrode potential as the local environment of cations in electrolytes is changed.

Diverse conductive frameworks have been implemented to Na-metal anodes to regulate the Na nucleation. Different frameworks have different sodiophilicity and therefore induce varied nucleation and deposition overpotentials. The influence of anode substrates on regulating Na nucleation and deposition overpotential was also not considered in the current contribution. Liu et al. reported that Na^+ has a lower reduction potential than Li^+ in carbonate electrolytes.[44] The observed Na deposition potential is about −0.54 V versus Na/Na^+, which is much lower than other studies under a similar deposition current density. While the observed Li deposition potential is about −0.13 V versus. Li/Li^+, which agrees with other reports. Therefore, other kinetic issues, including nucleation and deposition overpotential, can regulate the deposition trend of multications in electrolytes. These factors vary from case to case and are too complicated to be included in our current model.

In conclusion, based on the ion-solvent chemistry, a paradigmatic and rational strategy of the cation additive to stabilize electrolyte-anode interface for Na-metal batteries was established through first-principles calculations, MD simulations, FEM simulations, *in situ* optical microscopic observations, and electrochemical tests. Three principles of designing cation additives were proposed, including the

electrode potential, the LUMO level decrease of solvents, and the binding energy with solvents. Li^+ was predicted to the stabilize DME electrolytes on Na-metal anodes and also resist the growth of Na dendrites due to electrostatic shield effect. The role of electrolyte solvation was highlighted. The prediction was validated by *in situ* optical microscopic observations of Na nucleation on Cu wire and electrochemical tests. Such demonstrated strategy is also generalized into other rechargeable batteries, especially hybrid ion batteries. Therefore, cation additive strategy provides a new chance for electrolyte rational design to build a safe and stable battery.

EXPERIMENTAL PROCEDURES

Resource Availability

Lead Contact

Further information and requests for resources and reagents should be directed to and will be fulfilled by the Lead Contact, Professor Qiang Zhang (zhang-qiang@mails.tsinghua.edu.cn).

Materials Availability

This study did not generate new reagent nor materials. All materials used in this work are commercially available.

Data and Code Availability

The published article includes all datasets generated or analyzed during this study.

First-Principles Calculations

The first-principles calculations were conducted in Gaussian (G09)[45] program with Becke's three-parameter hybrid method using the Lee-Yang-Parr correlation functional (B3LYP) at 6-311G++G(d, p) level.[46] The solvation effect was considered with integral equation formalism variant of the Polarizable Continuum (IEFPCM) model.[47,48] The dielectric constant and solvent radius were set to be 7.2 and 4.19 Å for DME, respectively. Frequency analysis was performed to further confirm the ground state of cation-solvent complexes. As the interaction between DME molecules is very weak, the binding energy (E_b) between cations and solvents is defined as following:

$$E_b = E_{Complex} - E_M - n \times E_{DME}$$

where $E_{Complex}$ is the total energy of cation-solvent complex, E_M the total energy of cation, E_{DME} the total energy of DME, and n the number of DME in the complex.

For the calculation of theoretical electrode potential, zero-point correction and thermal correction to Gibbs free energy were adopted. As shown in Figure 1J, the stripping of metal was divided into three processes: the sublimation from solid to atoms, the ionization of atoms in vacuum, and the formation of solvated ions. Therefore, the energy change from bulk metal to solvated metal cations ($\Delta\varepsilon$) can be calculated by:

$$\Delta\varepsilon = \varepsilon_{cohe} + \varepsilon_{ion} + \varepsilon_{sol}$$

where ε_{cohe} is the cohesive energy, ε_{ion} the ionization energy, and ε_{sol} the solvation energy. Only the first item adopted experimental data,[49] and the latter two items used calculated data. Therefore, $\Delta\varepsilon$ can be further represented by:

$$\Delta\varepsilon = \varepsilon_{cohe}^{exp} + \varepsilon[M^{n+}] - \varepsilon[M] + \varepsilon[M(DME)_3^{n+}] - \varepsilon[M^{n+}] - 3\times\varepsilon[DME]$$

$$=\varepsilon_{cohe}{}^{exp} + \varepsilon[M(DME)_3{}^{n+}] - \varepsilon[M] - 3\times\varepsilon[DME]$$

Molecular Dynamics Simulations

Four electrolyte models were considered during MD simulations, including 0.50 M $NaPF_6$ DME, 1.00 M $NaPF_6$ DME, 1.00 M $NaPF_6$ + 0.50 M $LiPF_6$ DME, and 1.50 M $NaPF_6$ DME. The size of the cell is about 47×47×47 $Å^3$, which contains 616 DME molecules. The 1.00 M salt concentration is achieved by adding 64 $LiPF_6$ or $NaPF_6$ molecules. The MD simulations were performed in the Forcite module in Materials Studio of Accelrys Inc. with a condensed-phase optimized molecular potentials for atomistic simulation studies (COMPASS II) force field.[50] The time step and temperature were set to be 1 fs and 298 K, respectively. The electrolyte cells were firstly equilibrated in the isothermal-isobaric ensemble (NPT) using the Berendsen barostat to maintain the pressure of 0.1 GPa with a decay constant of 0.1 ps for 2,000 ps. The temperature was controlled by Nose thermostat. Then the production runs of another 2,000 ps were conducted in the canonical ensemble (NVT) at 298 K. Structural information were acquired every 0.20 ps to calculate the averaged radial distribution function and mean square displacement profile. The self-diffusion coefficient (D) was calculated according to the linear region of the mean square displacement profile by:

$$D = \frac{1}{6}\frac{\langle(\delta r)^2\rangle}{\Delta t}$$

Finite Element Method Simulations

The modeling of Na electrodeposition was performed by using COMSOL Multiphysics 5.4 based on the finite element method. Nernst-Planck-Possion equation was adopted to describe the behaviors of charged ions. The concentration-dependent Bulter-Volmer equation was employed to introduce the reaction of electrode surface. Deformed geometry interfaces were applied to the anode and cathode interface and the moving speed of meshes was equal to the deposited rate. The initial concentration of Na^+ was set to 1.0 mol L^{-1}. The exchange current density was set to be 30 A m^{-2}. The operation voltage was 0.40 V and the time of deposition was 20 s. For modeling the electrostatic shield effect induced by cation additives, the exchange current density was correlated to the intensity of electric field. Before simulation, a semiellipse nucleus was set.

In situ Optical Microscopic Observations

The *in situ* optical microscopic observations of Na plating were performed in a home-made cell (Figure 3C). A quartz was employed as cell body on account of its good corrosion resistance and high transparency. Silica gel was used for sealing. Tiny Na electrodes (counter electrode and reference electrode) were created by dipping Cu needle in molten Na. The assembly of the optical cell was conducted in an argon glovebox with both H_2O and O_2 less than 0.10 ppm. Then the cell was transferred and installed on object stage. Electrochemical workstation (Solartron 1470E) was adopted to apply a constant current (3.0 mA cm^{-2}). Images and videos were recorded by a metallurgical microscope with charge-coupled device (CCD) camera.

Electrochemical Tests

Na | Cu half cells were employed to evaluate the Coulombic efficiency and voltage hysteresis. CR2032 coin cell was assembled with Na metal electrode, 60-μL electrolyte, two-layer Celgard 2400, and Cu electrode. The electrolytes were 0.8 M $NaPF_6$ (MREDA) in DME (Alfa Aesar) and 0.8 M $NaPF_6$ + 0.4 M $LiPF_6$ (Tokyo Chemical Industry Co., Ltd.) in DME. The assembly process of cells and preparation of electrolytes

were carried out in an Argon-filled glove box. Cells were tested by a LAND multi-channel battery cycler (Wuhan LAND electronics Co., Ltd.).

SUPPLEMENTAL INFORMATION

Supplemental Information can be found online at https://doi.org/10.1016/j.chempr.2020.06.036.

ACKNOWLEDGMENTS

This work was supported by the National Key Research and Development Program (2016YFA0202500 and 2016YFA0200102) and the National Natural Scientific Foundation of China (21676160, 21825501, and 21808121). The authors acknowledged the support from Tsinghua National Laboratory for Information Science and Technology for theoretical simulations. We thank Xin-Bing Cheng for the helpful discussions.

AUTHOR CONTRIBUTIONS

Q.Z. conceived the study and supervised this work. X.C. and Q.Z. proposed the concept. X.C. carried out the DFT and MD calculations, while T.H. helped analyze the results. X.S. carried out the FEM calculations and experimental tests. R.Z. helped analyze the FEM results. X.C. and Q.Z. wrote the paper. T.H. and H.-J.P. helped revise the paper. All authors contributed to the discussion.

DECLARATION OF INTERESTS

The authors declare no competing interests.

Received: January 6, 2020
Revised: February 5, 2020
Accepted: June 28, 2020
Published: July 30, 2020

REFERENCES

1. Armand, M., and Tarascon, J.M. (2008). Building better batteries. Nature *451*, 652–657.

2. Canepa, P., Sai Gautam, G., Hannah, D.C., Malik, R., Liu, M., Gallagher, K.G., Persson, K.A., and Ceder, G. (2017). Odyssey of multivalent cathode materials: open questions and future challenges. Chem. Rev. *117*, 4287–4341.

3. Chen, X., Hou, T., Persson, K.A., and Zhang, Q. (2019). Combining theory and experiment in lithium–sulfur batteries: current progress and future perspectives. Mater. Today *22*, 142–158.

4. Cheng, X.B., Zhang, R., Zhao, C.Z., and Zhang, Q. (2017). Toward safe lithium metal anode in rechargeable batteries: a review. Chem. Rev. *117*, 10403–10473.

5. Lee, B., Paek, E., Mitlin, D., and Lee, S.W. (2019). Sodium metal anodes: emerging solutions to dendrite growth. Chem. Rev. *119*, 5416–5460.

6. Zhao, Y., Adair, K.R., and Sun, X. (2018). Recent developments and insights into the understanding of Na metal anodes for Na-metal batteries. Energy Environ. Sci. *11*, 2673–2695.

7. Tian, Y., Sun, Y., Hannah, D.C., Xiao, Y., Liu, H., Chapman, K.W., Bo, S.-H., and Ceder, G. (2019). Reactivity-guided interface design in Na metal solid-state batteries. Joule *3*, 1037–1050.

8. Zhang, Z., Ramos, E., Lalère, F., Assoud, A., Kaup, K., Hartman, P., et al. (2018). $Na_{11}Sn_2PS_{12}$: a new solid state sodium superionic conductor. Energy Environ. Sci. *11*, 87–93.

9. Zhou, W., Li, Y., Xin, S., and Goodenough, J.B. (2017). Rechargeable sodium all-solid-state battery. ACS Cent. Sci. *3*, 52–57.

10. Wang, S., Xu, H., Li, W., Dolocan, A., and Manthiram, A. (2018). Interfacial chemistry in solid-state batteries: formation of interphase and its consequences. J. Am. Chem. Soc. *140*, 250–257.

11. Cheng, E.J., Sharafi, A., and Sakamoto, J. (2017). Intergranular Li metal propagation through polycrystalline $Li_{6.25}Al_{0.25}La_3Zr_2O_{12}$ ceramic electrolyte. Electrochim. Acta *223*, 85–91.

12. Li, Q., Yi, T., Wang, X., Pan, H., Quan, B., Liang, T., Guo, X., Yu, X., Wang, H., Huang, X., et al. (2019). In-situ visualization of lithium plating in all-solid-state lithium-metal battery. Nano Energy *63*, 103895.

13. Ren, Y., Shen, Y., Lin, Y., and Nan, C.-W. (2015). Direct observation of lithium dendrites inside garnet-type lithium-ion solid electrolyte. Electrochem. Commun. *57*, 27–30.

14. Gao, L., Chen, J., Liu, Y., Yamauchi, Y., Huang, Z., and Kong, X. (2018). Revealing the chemistry of an anode-passivating electrolyte salt for high rate and stable sodium metal batteries. J. Mater. Chem. A *6*, 12012–12017.

15. Seh, Z.W., Sun, J., Sun, Y., and Cui, Y. (2015). A highly reversible room-temperature sodium metal anode. ACS Cent. Sci. *1*, 449–455.

16. Han, M., Zhu, C., Ma, T., Pan, Z., Tao, Z., and Chen, J. (2018). In situ atomic force microscopy study of nano–micro sodium deposition in ester-based electrolytes. Chem Commun (Camb). *54*, 2381–2384.

17. Lee, Y., Lee, J., Lee, J., Kim, K., Cha, A., Kang, S., Wi, T., Kang, S.J., Lee, H.W., and Choi, N.S. (2018). Fluoroethylene carbonate-based electrolyte with 1 M sodium bis(fluorosulfonyl) imide enables high-performance sodium metal electrodes. ACS Appl. Mater. Interfaces *10*, 15270–15280.

18. Rodriguez, R., Loeffler, K.E., Nathan, S.S., Sheavly, J.K., Dolocan, A., Heller, A., and Mullins, C.B. (2017). In situ optical imaging of sodium electrodeposition: effects of fluoroethylene carbonate. ACS Energy Lett. *2*, 2051–2057.

19. Ferdousi, S.A., Hilder, M., Basile, A., Zhu, H., O'Dell, L.A., Saurel, D., Rojo, T., Armand, M., Forsyth, M., and Howlett, P.C. (2019). Water as an effective additive for high-energy-density Na metal batteries? Studies in a superconcentrated ionic liquid electrolyte. ChemSusChem *12*, 1700–1711.

20. Jo, C.-H., Choi, J.U., Yashiro, H., and Myung, S.-T. (2019). Controllable charge capacity by using a black additive of high-energy-density sodium-ion battery. J. Mater. Chem. A *7*, 3903–3909.

21. Wang, H., Wang, C., Matios, E., and Li, W. (2018). Facile stabilization of the sodium metal anode with additives: unexpected key role of sodium polysulfide and adverse effect of sodium nitrate. Angew. Chem. Int. Ed. Engl. *57*, 7734–7737.

22. Ding, F., Xu, W., Graff, G.L., Zhang, J., Sushko, M.L., Chen, X., Shao, Y., Engelhard, M.H., Nie, Z., Xiao, J., et al. (2013). Dendrite-free lithium deposition via self-healing electrostatic shield mechanism. J. Am. Chem. Soc. *135*, 4450–4456.

23. Chen, X., Li, H.R., Shen, X., and Zhang, Q. (2018). The origin of the reduced reductive stability of ion–solvent complexes on alkali and alkaline earth metal anodes. Angew. Chem. Int. Ed. Engl. *57*, 16643–16647.

24. Chen, X., Shen, X., Li, B., Peng, H.J., Cheng, X.B., Li, B.Q., Zhang, X.Q., Huang, J.Q., and Zhang, Q. (2018). Ion–solvent complexes promote gas evolution from electrolytes on a sodium metal anode. Angew. Chem. Int. Ed. Engl. *57*, 734–737.

25. Chen, X., Hou, T.-Z., Li, B., Yan, C., Zhu, L., Guan, C., Cheng, X.-B., Peng, H.-J., Huang, J.-Q., and Zhang, Q. (2017). Toward stable lithium–sulfur batteries: mechanistic insights into electrolyte decomposition on lithium metal anode. Energy Storage Mater. *8*, 194–201.

26. Komaba, S., Hasegawa, T., Dahbi, M., and Kubota, K. (2015). Potassium intercalation into graphite to realize high-voltage/high-power potassium-ion batteries and potassium-ion capacitors. Electrochem. Commun. *60*, 172–175.

27. Kubota, K., Dahbi, M., Hosaka, T., Kumakura, S., and Komaba, S. (2018). Toward K-Ion and Na-Ion batteries as "beyond Li-Ion. Chem. Rec. *18*, 459–479.

28. Kalapsazova, M., Rasheev, H., Zhecheva, E., Tadjer, A., and Stoyanova, R. (2019). Insights into the function of electrode and electrolyte materials in a hybrid lithium–sodium ion cell. J. Phys. Chem. C *123*, 11508–11521.

29. Borodin, O., Giffin, G.A., Moretti, A., Haskins, J.B., Lawson, J.W., Henderson, W.A., and Passerini, S. (2018). Insights into the structure and transport of the lithium, sodium, magnesium, and zinc bis(trifluoromethansulfonyl)imide salts in ionic liquids. J. Phys. Chem. C *122*, 20108–20121.

30. Cresce, A.V., Russell, S.M., Borodin, O., Allen, J.A., Schroeder, M.A., Dai, M., Peng, J., Gobet, M.P., Greenbaum, S.G., Rogers, R.E., and Xu, K. (2016). Solvation behavior of carbonate-based electrolytes in sodium ion batteries. Phys. Chem. Chem. Phys. *19*, 574–586.

31. Doyle, K.P., Lang, C.M., Kim, K., and Kohl, P.A. (2006). Dentrite-free electrochemical deposition of Li–Na alloys from an ionic liquid electrolyte. J. Electrochem. Soc. *153*, A1353–A1357.

32. Liyana-Arachchi, T.P., Haskins, J.B., Burke, C.M., Diederichsen, K.M., McCloskey, B.D., and Lawson, J.W. (2018). Polarizable molecular dynamics and experiments of 1,2-dimethoxyethane electrolytes with lithium and sodium salts: structure and transport properties. J. Phys. Chem. B *122*, 8548–8559.

33. Fan, X., Gaddam, R.R., Kumar, N.A., and Zhao, X.S. (2017). A hybrid Mg^{2+}/Li^{+} battery based on interlayer-expanded MoS_2/graphene cathode. Adv. Energy Mater. *7*, 1700317.

34. Li, M., He, Q., Li, Z., Li, Q., Zhang, Y., Meng, J., et al. (2019). A novel dendrite-free Mn^{2+}/Zn^{2+} hybrid battery with 2.3 V voltage window and 11000-cycle lifespan. Adv. Energy Mater. *9*, 1901469.

35. Zhang, L., Zhang, C., Ding, Y., Ramirez-Meyers, K., and Yu, G. (2017). A low-cost and high-energy hybrid iron-aluminum liquid battery achieved by deep eutectic solvents. Joule *1*, 623–633.

36. Zhang, Z., Zhao, M., Xia, M., Qi, R., Liu, M., Nie, J., Wang, Z.L., and Lu, X. (2018). Magnesium anodes with extended cycling stability for lithium-ion batteries. Adv. Funct. Mater. *29*, 1806400.

37. Chen, X., Zhang, X.-Q., Li, H.-R., and Zhang, Q. (2019). Cation–solvent, cation–anion, and solvent–solvent interactions with electrolyte solvation in lithium batteries. Batteries & Supercaps *2*, 128–131.

38. Davidson, R., Verma, A., Santos, D., Hao, F., Fincher, C., Xiang, S., Van Buskirk, J., Xie, K., Pharr, M., Mukherjee, P.P., and Banerjee, S. (2019). Formation of Magnesium dendrites during electrodeposition. ACS Energy Lett. *4*, 375–376.

39. Hou, T., Yang, G., Rajput, N.N., Self, J., Park, S.-W., Nanda, J., and Persson, K.A. (2019). The influence of FEC on the solvation structure and reduction reaction of LiPF6/EC electrolytes and its implication for solid electrolyte interphase formation. Nano Energy *64*, 103881.

40. Qian, J., Henderson, W.A., Xu, W., Bhattacharya, P., Engelhard, M., Borodin, O., and Zhang, J.G. (2015). High rate and stable cycling of lithium metal anode. Nat. Commun. *6*, 6362.

41. Wang, J., Yamada, Y., Sodeyama, K., Watanabe, E., Takada, K., Tateyama, Y., and Yamada, A. (2018). Fire-extinguishing organic electrolytes for safe batteries. Nat. Energy *3*, 22–29.

42. Zeng, Z., Murugesan, V., Han, K.S., Jiang, X., Cao, Y., Xiao, L., Ai, X., Yang, H., Zhang, J.-G., Sushko, M.L., and Liu, J. (2018). Non-flammable electrolytes with high salt-to-solvent ratios for Li-ion and Li-metal batteries. Nat. Energy *3*, 674–681.

43. Zheng, J., Chen, S., Zhao, W., Song, J., Engelhard, M.H., and Zhang, J.-G. (2018). Extremely stable sodium metal batteries enabled by localized high-concentration electrolytes. ACS Energy Lett. *3*, 315–321.

44. Liu, J., Wang, Y., Liu, F., Cheng, F., and Chen, J. (2020). Improving metallic lithium anode with $NaPF_6$ additive in LiPF6-carbonate electrolyte. J. Energy Chem. *42*, 1–4.

45. Frisch, M., J., Trucks, G., W., Schlegel, H., B., Scuseria, G., E., Robb, M., A., Cheeseman, J., R., et al. (2016). Gaussian 09, Revision A.02 (Gaussian, Inc.).

46. Becke, A.D. (1993). Density-functional thermochemistry. III. The role of exact exchange. J. Chem. Phys. *98*, 5648–5652.

47. Cancès, E., Mennucci, B., and Tomasi, J. (1997). A new integral equation formalism for the polarizable continuum model: theoretical background and applications to isotropic and anisotropic dielectrics. J. Chem. Phys. *107*, 3032–3041.

48. Miertuš, S., Scrocco, E., and Tomasi, J. (1981). Electrostatic interaction of a solute with a continuum. A direct utilizaion of ab initio molecular potentials for the prevision of solvent effects. Chem. Phys. *55*, 117–129.

49. Kaxiras, E. (2003). Atomic and Electronic Structure of Solids (Cambridge University Press).

50. Sun, H. (1998). COMPASS: an ab initio force-field optimized for condensed-phase applications overview with details on alkane and benzene compounds. J. Phys. Chem. B *102*, 7338–7364.